Electrochemical and Solid-State Letters, **11** (8) K73-K77 (2008)
1099-0062/2008/11(8)/K73/5/$23.00 © The Electrochemical Society

Structural and Nonlinear Optical Properties of Self-Assembled SnO_2-Doped Silicon Nanorings Formed by Pulsed Laser Ablation

J. R. Rani,[a,z] V. P. Mahadevan Pillai,[a] C. S. Suchand Sandeep,[b] and Reji Philp[b]

[a]*Department of Optoelectronics, University of Kerala, Kariavattom, Trivandrum, Kerala, 695 581 India*
[b]*Light and Matter Physics Group, Raman Research Institute, Bangalore, 560 080 India*

SnO_2-doped Si nanorings with an outer diameter of 25 nm and an average width of 5 nm are grown by pulsed laser deposition. Atomic force microscopy reveals several interesting self-assembling forms of polycrystalline as well as an amorphous type of silicon nanorings. Depending on the width of the ring, the optical bandgap and photoluminescence can be tuned from the near infrared (1.38 eV) to the ultraviolet (3.02 eV), giving evidence for the strong quantum confinement effect along the width of ringlike quantum states. From Z-scan studies, the two-photon absorption coefficient is determined to be 2.2×10^{-6} m/W.
 [DOI: 10.1149/1.2928841]

Manuscript submitted December 4, 2007; revised manuscript received March 9, 2008. Available electronically May 19, 2008.

The physical, optical, and electronic properties of materials become dependent on their shapes when their size is reduced to nanoscale dimensions.[1] Several shapes including prisms, disks, stars, cubes, rods, and rings have been synthesized, and their basic properties characterized.[2] Nanorings, the latest member of the nanoscale structures, which are artificial clusters that strongly confine electrons in three dimensions, are a growing area of research due to their unique physical properties of possible tunable electronic states,[3] and high oscillator strength for the ground-state band-to-band transition.[4] Recently, Hobbs and co-workers reported the fabrication of Si nanorings (Si NRs).[5] In the presence of coulomb correlation, the so-called Aharonov–Bohm effect of excitons[6] exists in small NRs with a typical inner and outer radius of 20 and 100 nm, respectively, and a height of 2–3 nm, which can strongly confine carriers into ringlike quantum states.[7] In the present work we discuss the formation and characterization of ring-shaped nanostructures of silicon doped with tin oxide, formed by pulsed laser deposition. Si–Sn alloy is a group IV system in which Sn is highly substitutional to Si, with promising applications in the communication wavelength range.[8] However, investigations on SnO_2-doped Si NRs have been scarce.

In our experiment, tin oxide (3 wt %)-doped Si pellets sintered at 1330°C were used as the target material, and single crystals of sapphire were used as the substrate. The deposition was carried out by the off-axis pulsed laser deposition (PLD) method,[9] with and without background Ar gas (0.001–0.15 mbar). A Q-switched, frequency-doubled pulsed Nd:yttria aluminum garnet laser (532 nm, 210 mJ energy, 7 ns pulse width, and 10 Hz repetition frequency) was used to ablate the target. A lens of focal length 20 cm was used to focus the laser beam into the chamber. The substrates were kept at a target to substrate distance of 5 mm, at a 5 cm off-axis position with respect to the laser plume. Photoluminescence (PL) spectra of the films were recorded [JobinYvon Spectrofluorometer (Fluorolog III)] with an excitation of 350 nm. The nanoscale structures of the films were examined by a Hitachi H–600 transmission electron microscope (TEM) and an atomic force microscope (AFM) (Digital Instruments, Nanoscope III). Z-scan experiments were performed using the laser mentioned above at a pulse energy of 7 μJ. The crystal structure was examined using an X-ray diffractometer (Rigaku) with Cu Kα ($\lambda = 1.5418$ Å) radiation. X-ray photoelectron spectroscopy (XPS) was carried out by extreme ultraviolet beamline of Indus 1. Energy-dispersive spectroscopy (EDS) was done by a JEOL JSM–5600 LV scanning electron microscope.

Figure 1 shows the AFM images of the as-deposited NRs. The variation of ring diameter with Ar pressure is shown in Table I. A number of oval-shaped rings were self-assembled on a sapphire substrate without background Ar gas (Fig. 1a). The formation of the ring pattern is a complicated process, where the interparticle interaction plays a role in deciding the nature of the pattern. In most cases the kinetic energy of the deposited atoms was on the order of 5 eV, and thus below the threshold for sputtering, which is around 10–25 eV.[10] Previous reports indicate the significance of self-sputtering (resputtering) effects[11] during PLD, which plays a dominant role for the high-energy particles. In our case the laser fluence was very high (25 J/cm^2). It was found that, at high laser fluences, a significant fraction of the SnO_2-doped silicon atoms deposited on the substrate was sputtered from that substrate due to the bombardment of high-energy particles in the incoming flux of atoms and ions. The amount of resputtered material should depend on the ionized fraction of the ablated particles. Resputtering from the center of the dots resulted in a distinct depression in the center, which formed ringlike quantum structures, but some material still remained in the middle. Barnes et al.[12] reports the formation of hollow, shell-like particles due to resputtering in PLD, and the TEM observation in their study has some similarities to the present study. They report that, with increasing the energy density, resputtering increases and the shapes of the nanoparticles (NPs) are also modified. The NP size increases in the out-of-plane direction and the NPs retain a roughly circular in-plane shape. The streaking is strongest at the center of the NPs, giving them a pointed shape. This leads to a reshaping of the NPs, elongating them in the growth direction. Thus, there is more material in the center of the NPs. In some cases cavities are formed in the NPs, which are caused by local melting that result in mass redistribution. A similar explanation is given by Hofmeister,[13] who suggests that the melting can start from the inside of the NP, with the molten metal being ejected and leaving a hollow shell. The shape of the rings drastically changes from oval to circular when the depositions are made in Ar ambience (Fig. 1b-d). The size distribution is not uniform for all samples, showing a clear anisotropy in the redistribution. The presence of the background gas during irradiation fundamentally changes the mechanism for NP formation.[14] Experiments and multiple-scattering simulations show that heavier Ar atoms effectively remove Si atoms from the forward-going flux, and can even scatter Si atoms backward, and in all instances the background gas appears to act as a regulator of ablated plume energetics.[14] At a pressure of the order of 0.001 mbar, the mean-free path is approximately 5 cm,[14] which becomes 0.05 cm at a higher pressure of 0.133 mbar. In our case the pressure is very low and the average mean-free path is comparable to the target to substrate distance (5 cm), which will decrease the collisions. This can help the deposition of small particles as well as increase the resputtering effects. As the pressure increases to 0.15 mbar, the average value of the mean-free path decreases and more collisions can occur between the ejected species and buffer gas atoms before reaching the substrate. This compresses the ambient gas to such an extent that a

[z] E-mail: ranijnair@rediffmail.com

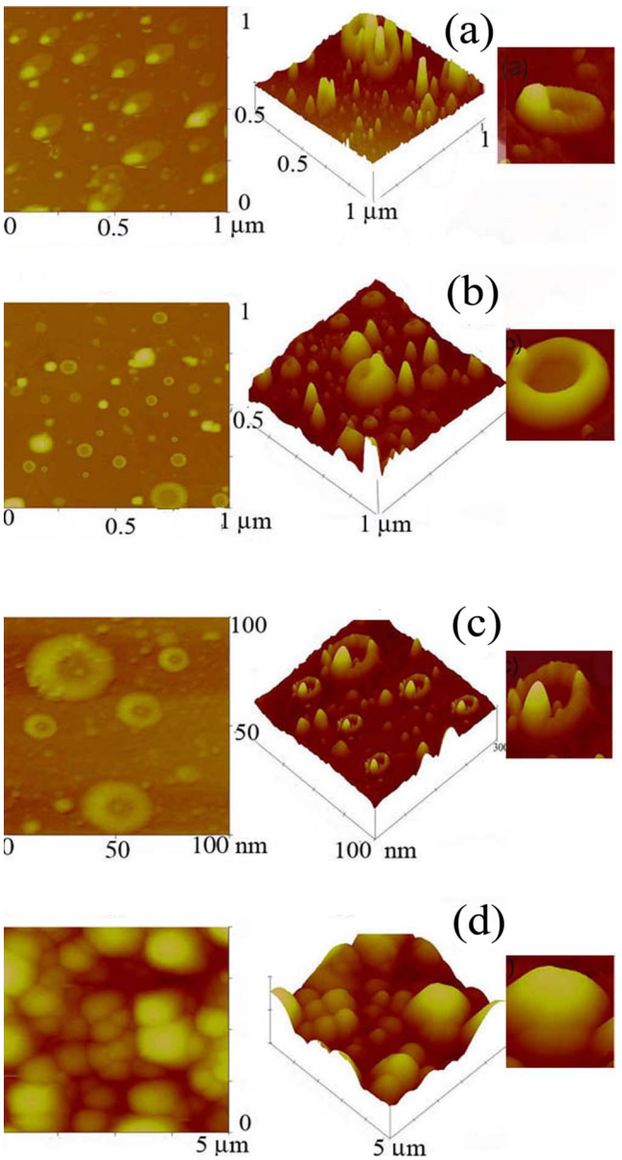

Figure 1. (Color online) Two-dimensional (left column) and three-dimensional (middle column) AFM images of tin oxide-doped Si NRs deposited (a) without any ambient gas and with Ar ambient of partial pressures of (b) 0.001, (c) 0.009, and (d) 0.15 mbar. Close-up view of a single ring is shown in the right column.

shock wave develops, and the transformation of plume kinetic energy into thermal energy takes place. Thus, resputtering effects are suppressed (Fig. 1d) due to a rise in the background pressure, which results in a low kinetic energy of the species in the plume due to their intensive collisions with gas atoms or molecules. Vapor species can undergo enough collisions so that nucleation and growth of these vapor species to form particles can occur before their arrival at the substrate, and the residence time of the particles in the vapor controls its size.[14] The longer the residence time, as is the case with increased ambient gas pressure, the larger the size of the particles.[14] A high ambient gas pressure results in a sharpening of the plume boundary and a slowing of the plume relative to the propagation in vacuum, which results in a spatial confinement of the plume.

In our case the laser fluence was 25 J/cm^2. Previous reports show that in this laser fluence resputtering effects take place.[15,16] Barnes et al. report the formation of hollow, shell-like particles due to resputtering in PLD, and the TEM observation in their study has similarities with the present study.[15] They report that, with increasing energy density, resputtering increases and the shapes of the NPs are also modified. The NP size increases in the out-of-plane direction and the NPs retain a roughly circular in-plane shape. The streaking is strongest at the center of the NPs, giving them a pointed shape. This leads to a reshaping of the NPs, elongating them in the growth direction and in some cases forming cavities in the NPs. In the present case, as the Ar pressure increases (0.11 mbar), the formation of ringlike structures vanishes, which shows that resputtering plays a key role for the formation of ringlike structures. EDS analysis shows that NRs consist of Si, Sn, and O_2. The same weight percentage of Sn as that in the target was found in all films (3 wt %).

Table I. Physical and optical properties of the NRs under different background Ar pressures.

Ar pressure (mbar)	Outer diameter (nm)	Average width of ring (nm)	Bandgap (eV)	PL peak energy (eV)
0	100–170	25	2.19	2
0.002	60–120	12	2.85	2.77
0.009	25–60	7	3.15	2.99

The X-ray diffraction (XRD) pattern of the SnO_2-doped Si pellets sintered at 1350°C (Fig. 2) shows all the major peaks of microcrystalline silicon with a shift of 0.97° to the higher 2θ value, which results in decreasing d values for all the planes. For doped pellets the value of the lattice constant is found to be 5.33 Å, while for undoped Si it is 5.43 Å. However, the broadening of the full width at half-maximum of the XRD peaks of the SnO_2-doped Si with reference to Si pellet shows the incorporation of Sn in the Si lattice and the contraction of the host lattice.[17] Sintering of the pellets at 1350°C can favor the formation of SiO_2 and SnO_2.[18] The TEM image of the rings deposited at 0.002 mbar Ar (inset of Fig. 2) shows that the rings are nearly circular in shape and can be classified into a small number of sizes with the outer diameter varying from 50 to 100 nm and an average wall width of 10 nm. The selected area electron diffraction (SAED) pattern of the sample confirms that the film is made of many small crystalline as well as amorphous particles. When the NR diameter is greater than 70 nm, the rings are more polycrystalline in nature, with different grain orientations, and

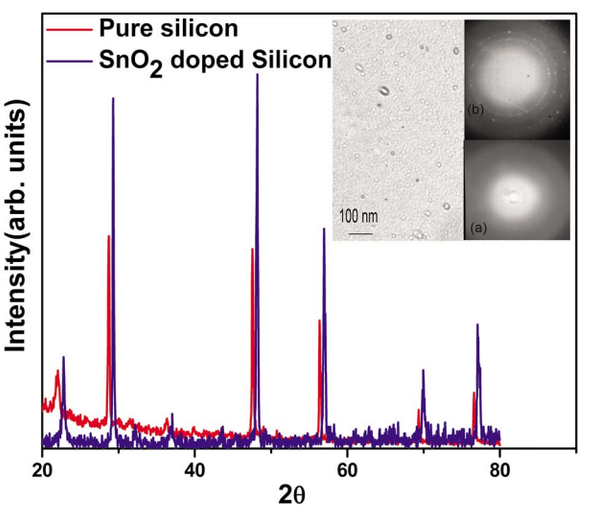

Figure 2. (Color online) XRD pattern of pure Si and SnO_2-doped silicon pellets. Inset shows TEM image of SnO_2-doped samples deposited with an Ar pressure of 0.002 mbar. The SAED pattern of the rings of outer diameter (a) 25 and (b) 50 nm also are shown.

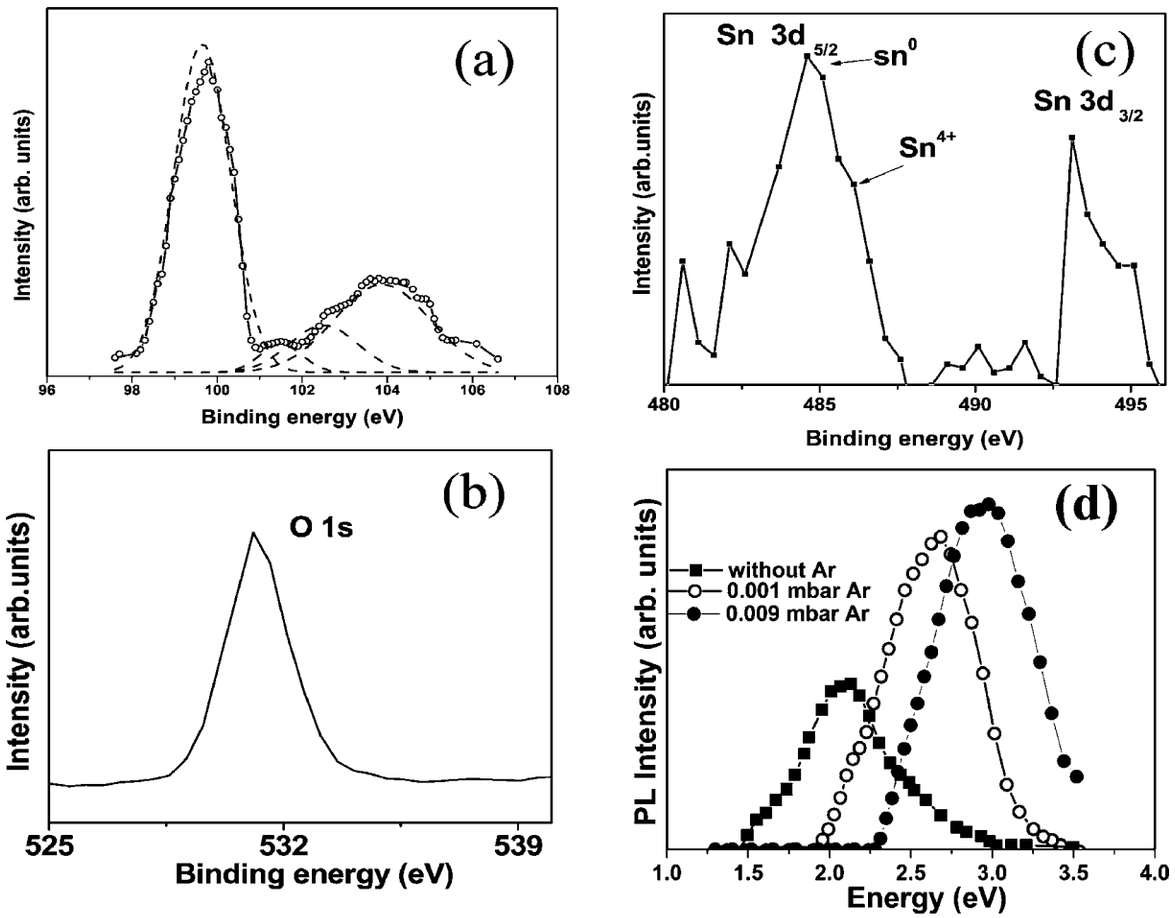

Figure 3. XPS core-level spectra of the NRs deposited at 0.001 mbar Ar pressure. (a) Si $2p_{3/2}$ region, (b) O 1s region, and (c) Sn 3d region. PL spectra of the NRs deposited with different Ar background gas pressures are shown in (d).

the grain sizes have a dispersive distribution. But, rings with 50–70 nm size with the highly diffuse ring pattern indicate that the NRs are amorphous Si, suggesting the formation of a medium-range order (Fig. 3c). The first four peaks from the center, with interlayer d-spacing of 3.0635, 1.8904, 1.6192, and 1.3451 Å, respectively, are indexed as (111), (220), (311), and (400). They are crystallized in face-centered cubic structure, with the lattice constant "a" as 5.3515 Å, which is consistent with XRD results. The chemical composition of the NRs is determined with EDS, which shows the presence of silicon, oxygen, and Sn; no evidence of other impurities has been detected (figure not shown).

Figure 3 shows the XPS spectra of the samples deposited at 0.003 mbar Ar pressure. All samples show the same XPS pattern. The XPS peak around 99.6 eV is the peak corresponding to Si $2p_{3/2}$. By the deconvolution of the Si_{2p} oxide spectrum, four possible oxidation states (Si^{+1}, Si^{+2}, Si^{+3}, and Si^{+4}) are obtained, which show energy shifts of 1.7 ± 0.01, 2.8 ± 0.015, 3.7 ± 0.02, and 4.7 ± 0.011 eV relative to the binding energy of Si $2p^0$, which is consistent with previous results.[19] The increasing electronegativity of the Si–O bond relative to the Si–Si bond results in a shift to higher binding energy of the core-level electrons in the Si. The O 1s signal is recorded at 532 eV at the surface of the layer, which is in fact the expected position characteristic of SiO_2, and a small hump at 533.5 eV is due to the O 1s level in SnO_2.[19] The thickness of the SiO_x layer can be calculated from the equation

$$t_{SiO_x} = \frac{\lambda_{SiO_x}}{\sqrt{2}} \times \ln\left(1 + \frac{\lambda_{si}}{r \times \lambda_{SiO_x}}\right) \quad [1]$$

where r is the ratio of the SiO_x peak area to the Si peak area and λ is the electron inelastic mean-free path. λ values for silicon species were obtained directly from the literature. λ is 30 Å for Si, and 36 Å for SiO_2.[20-22]

The thickness of the SiO_x layer is calculated and the physical thickness is $\sim$20 nm. The peak located at 484.72 eV is due to metallic Sn (Sn $3d_{5/2}$), and another peak at 486.95 eV is due to photoelectrons emitted from SnO_2 in which Sn has the +4 oxidation state.[20] Figure 3c shows the Sn $3d_{3/2}$ spectrum of the film exhibiting a weak peak at 493.1 eV, and the spin-orbit splitting of $3d_{5/2}$ and $3d_{3/2}$ lines is found to be 8.38 eV.[20]

Bandgap values are calculated from the absorption spectrum (not shown), and the PL spectrum is shown in Fig. 3d. The variation of the bandgap and PL peak with respect to the width of the ring is shown in Table I. Incorporation of Sn into the Si lattice changes its bandgap from indirect to direct at a concentration of about 20% Sn, and the Sn atoms occupy substitutional sites.[23] Depending on the size and the chemical environment, the bandgap of the silicon NPs can become as large as 2–3 eV due to quantum confinement, as revealed by some theoretical calculations and experimental results.[24,25] The blueshift of the PL peak from the bulk value (1.1 eV) and the absence of visible PL from the samples deposited at 0.15 mbar Ar further support our interpretation of the PL peak as

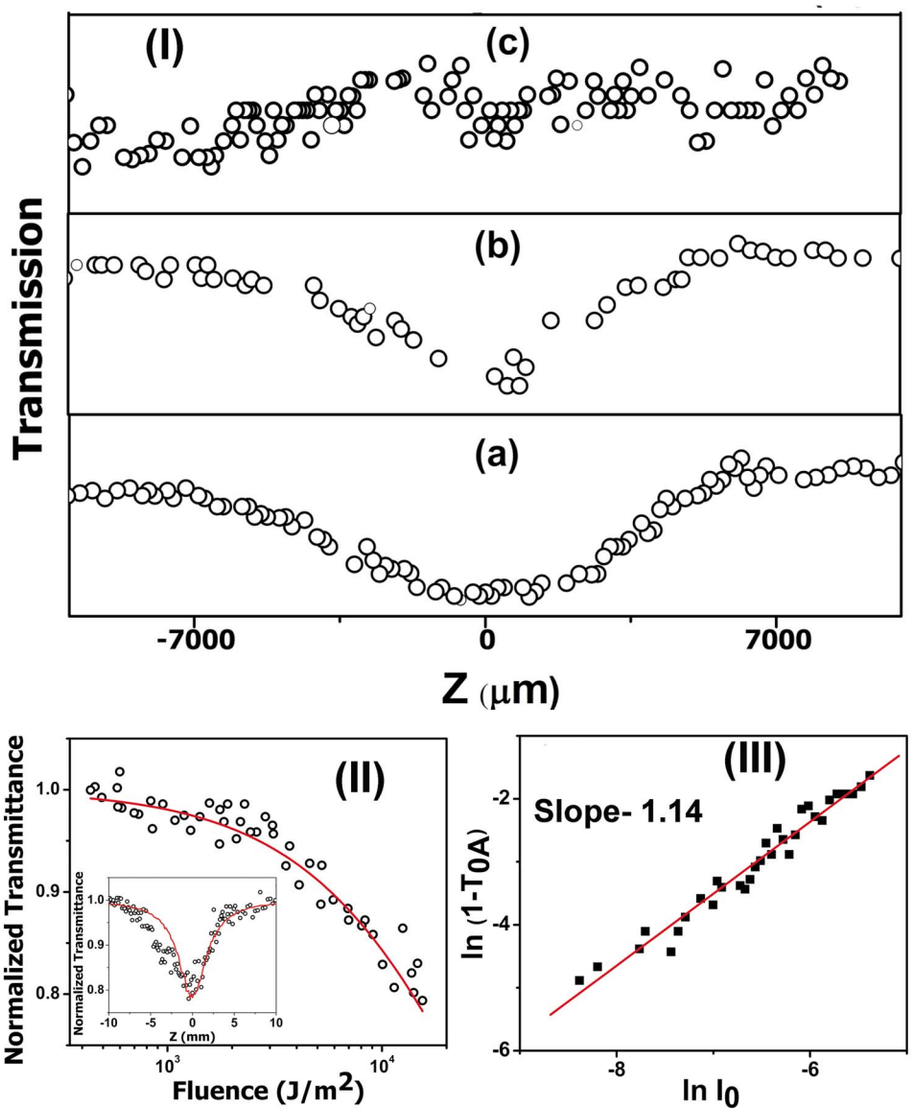

Figure 4. (Color online) (I) Open-aperture Z-scan measurements of the samples deposited under different Ar background gas pressures. (a) 0.001, (b) 0.009, and (c) 0.15 mbar. (II) Normalized transmittance of the sample deposited under 0.001 mbar Ar pressure, as a function of the input laser fluence. The data are obtained from the Z-scan data shown in the inset. Solid curves are theoretical fits to the experimental data (circles). (III) plot of $\ln(I_0)$ vs $\ln(1 - T_{OA})$. Solid line is the linear fit to the data.

representative of the bandgap, and the PL peak blueshift of Si NRs as due to the quantum confinement. Silicon nanocrystals with a size around 2–5 nm having the optical bandgap of 2.9 eV show a PL maximum at 2.9 eV due to the quantum confinement effect.[26] The bandgap value and PL peak energy increase as the width of the rings decreases from 25 to 7 nm, which shows that the confinement is along the width of the ring. In the 0.15 mbar deposited sample there is no ringlike structure. The size of the particle is very large. So, the possibility for confinement is very low. But, in other cases the ringlike structure appears and the width of the ring is below 10 nm. The confinement is along the width of the ring, which may result in PL in the visible region.

An open-aperture Z-scan experiment[27] can be used to measure the nonlinear optical absorption coefficient of the Si NRs (Fig. 4). For nanosecond laser fluences from 10^3 to 10^4 J/m^2, the experiments show a clear reverse saturable absorption behavior [Fig. 4(II)]. Fitting the experimental results to theory, the two-photon absorption (2PA) coefficient for the Si NRs at 532 nm is found to be 2.2×10^{-6} m/W. From the linear fit to the plots of $\ln(1 - T_{OA})$ vs $\ln(I_0)$, where T_{OA} is the normalized energy transmittance and I_0 is the excitation intensity, one finds the gradient to be ~ 1 [Fig. 4(III)], confirming 2PA.[28] Excitation of carriers at 4.6 eV, well above the indirect gap of Si NRs of 3 eV, creates a nonequilibrium carrier distribution that is expected to relax to the indirect bandedge via phonon emission. Shields et al.[29] experimentally show that, in silicon crystal, an excess photon energy of about 1.3 eV is given as kinetic energy to each electron–hole pair, and most of this energy is lost by subpicosecond emission of longitudinal orbital phonons. A similar situation is also reported for the Z-scan studies of Au–Ag alloy nanoclusters.[30]

In conclusion, SnO_2-doped Si NRs of size 20–50 nm have been grown on a sapphire substrate, and the self-sputtering process modifies the material distribution on the substrate, leading to the formation of ring-shaped structures. PL emission energy can be tuned into the visible range of light by controlling the sizes of the Si NRs, and the bandgap energy is blueshifted into the range of visible light owing to the quantum confinement effect along the width of the ring. Si NRs are promising candidates for visible, tunable, and high-efficiency light-emitting devices. The large optical nonlinearity of the NRs indicates that they can also find applications in optical limiting, switching, and modulated-type optical devices.

References

1. H. S. Kwok, H. S. Kim, D. H. Kim, W. P. Shen, X. W. Sun, and R. F. Xiao, *Appl. Surf. Sci.*, **595**, 109 (1997).
2. J. C. Hulteen, D. A. Treichel, M. T. Mith, M. L. Duval, T. R. Jensen, and R. P. Van Duyne, *J. Phys. Chem. B*, **103**, 3854 (1999).

3. J. M. Garcia, T. M. Mankad, P. O. Holtz, P. J. Wellman, and P. M. Petroff, *Appl. Phys. Lett.*, **72**, 1857 (2001).
4. H. Pettersson, R. J. Warburton, A. Lorke, K. Karrai, J. P. Kotthaus, J. M. Garcia, and P. M. Petroff, *Physica E (Amsterdam)*, **6**, 510 (2000).
5. K. L. Hobbs, P. R. Larson, G. D. Lian, J. C. Keay, and M. B. Johnson, *Nano Lett.*, **4**, 167 (2004).
6. A. Lorke, R. J. Luyken, A. O. Govorov, J. P. Kotthaus, J. M. Garcia, and P. M. Petroff, *Phys. Rev. Lett.*, **84**, 2223 (2000).
7. E. J. Preisler, O. J. Marsh, R. A. Beach, and T. C. McGilla, *J. Vac. Sci. Technol. B*, **19**, 1611 (2001).
8. A. M. Grundmann, O. Stier, and D. Bimberg, *Phys. Rev. B*, **52**, 11969 (1995).
9. J. R. Rani, R. S. Ajimsha, R. S. Jayasree, V. P. Mahadevan Pillai, and M. K. Jayaraj, *J. Appl. Phys.*, **100**, 014302 (2006).
10. S. Fahler and H. U. Krebs, *Appl. Surf. Sci.*, **61**, 96 (1996).
11. S. K. Hau, K. H. Wong, P. W. Chan, and C. L. Choy, *Appl. Phys. Lett.*, **66**, 245 (1995).
12. J.-P. Barnes, N. Beer, A. K. Petford-Long, A. Suarez-Garcıa, R. Serna, D. Hole, M. Weyland, and P. A. Midgley, *Nanotechnology*, **16**, 718 (2005).
13. H. Hofmeister, M. Dubiel, H. Graener, and J. C. Pivin, *Radiat. Eff. Defects Solids*, **158**, 49 (2003).
14. Li-Chyng Chen, in *Pulsed Laser Deposition of Thin Films*, D. B. Chrisey and G. K. Hubler, Editors, p. 186, Chap. 6, Wiley, New York (1994).
15. J.-P. Barnes, N. Beer, A. K. Petford-Long, A. Suarez-Garcıa, R. Serna, D. Hole, M. Weyland, and P. A. Midgley, *Nanotechnology*, **16**, 718 (2005).
16. H. Hofmeister, M. Dubiel, H. Graener, and J. C. Pivin, *Radiat. Eff. Defects Solids*, **158**, 49 (2003).
17. N. F. M. Henry, H. Lipson, and W. A. Wooster, *The Interpretation of X ray Diffraction Photographs*, p. 217, Macmillan & Co., New York (1960).
18. Y. H. Yano, G. F. Fenna, M. Kativar, N. Malev, and J. R. Abelson, *J. Vac. Sci. Technol. A*, **11**, 219 (1993).
19. F. J. Grunthaner and J. Maserjian, *IEEE Trans. Nucl. Sci.*, **NS-24**, 2108 (1977).
20. J. M. Themlin, M. Chtaib, L. Henrard, P. Lambin, J. Darville, and J. M. Gilles, *Phys. Rev. B*, **46**, 2460 (1992).
21. E. J. Preisler, O. J. Marsh, R. A. Beach, and T. C. McGilla, *J. Vac. Sci. Technol. B*, **19**, 1611 (2001).
22. S. Tanuma, C. Powell, and D. Penn, *Surf. Interface Anal.*, **11**, 577 (1988).
23. S. Yu. Shiryaev, J. L. Hansen, P. Kringhoj, and A. Nylandsted Larsen, *Appl. Phys. Lett.* **67**, 2287 (1995).
24. G. Allan, C. Delerue, and M. Lannoo, *Phys. Rev. Lett.*, **78**, 3161 (1997).
25. L. Y. Chen, W. H. Chen, and F. C. N. Hong, *Appl. Phys. Lett.*, **86**, 193506 (2005).
26. V. Svrcek, T. Sasaki, Y. Shimizu, and N. Koshizaki, *Appl. Phys. Lett.*, **89**, 213113 (2006).
27. M. Sheik-Bahae, A. A. Said, T. H. Wei, D. J. Hagan, and E. W. Van Stryland, *IEEE J. Quantum Electron.*, **26**, 760 (1990).
28. J. He, W. Ji, J. Mi, Y. Zheng, and J. Y. Ying, *Appl. Phys. Lett.*, **88**, 181114 (2006).
29. J. A. Shields and J. P. Wolfe, *Z. Phys. B: Condens. Matter*, **75**, 11 (1989).
30. R. Philip, G. Ravindra Kumar, N. Sandhyarani, and T. Pradeep, *Phys. Rev. B*, **62**, 13160 (2000).